ACOUSTIC TOMOGRAPHY OF THE ATMOSPHERE USING UNSCENTED KALMAN FILTER

Soheil Kolouri and Mahmood R. Azimi-Sadjadi

Colorado State University
Electrical and Computer Engineering Department
Fort Collins, CO, 80523-1373 USA
Email: azimi@engr.colostate.edu

ABSTRACT

Acoustic travel-time tomography of the atmosphere is a nonlinear inverse problem which attemps to reconstruct temperature and wind velocity fields in the atmospheric surface layer (ASL) using the dependence of sound speed on temperature and wind velocity fields along the propagation path. A new statistical-based algorithm is introduced in this paper based on fixed-point unscented Kalman filter (UKF) which is capable of reconstructing and tracking temperature and wind velocity fields within a specified investigation area.

Index Terms— Acoustic Tomography, Unscented Transform, Unscented Kalman Filter

1. INTRODUCTION

Monitoring temperature and wind velocity fields in the atmospheric surface layer has always been of great importance in different disciplines, such as boundary layer meteorology, and studies of wave propagation through a turbulent atmosphere. The conventional approach to measure these fields is to use in-situ thermo-anemometers. However employing these sensors within the investigation area has two major drawbacks. First, this is not an economically viable solution as a large number of such rather expensive sensors is needed to achieve an acceptable spatial resolution. Moreover, deploying these sensors in an investigation area may distort the measured fields and hence leading to inaccurate measurements.

Acoustic tomography [1] technique is a popular method [1, 2, 3] that has been used in order to measure temperature and wind velocity fields with minimal interference in the investigation area as well as lesser cost. Acoustic tomography's goal [1, 2, 3] is to estimate temperature and wind velocity fields in an investigation area given the characteristics of the sound sources, the coordinates of sensors and the travel time for acoustic propagation paths. In [1], the authors showed that using acoustic tomography is highly beneficial, as it uses a small number of acoustic sensors to reconstruct the temperature and wind velocity fields with high spatial resolution. Several other acoustic tomography methods have recently been introduced that can be categorized as statistical-based algorithms [1, 3], algebraic-based algorithms [2] and those which use sparse reconstruction framework [4]. Among the statistical-based methods are the stochastic inversion (SI) [1] and the time-dependent stochastic inversion (TDSI) [3] methods. The simultaneously iterative reconstruction technique (SIRT) in [2] belongs to the algebraic-based category.

In this paper, a new statistical-based approach toward solving the acoustic tomography problem is presented which casts the problem as a nonlinear state-estimation problem in which states represent the temperature and wind velocity fields in each grid over the monitored area. Unscented Kalman filter (UKF) [5] is employed to estimate and track these states at every time snapshot. UKF is based on Unscented Transform method which does not require linearization of the state or observation equations. The proposed method uses 3-D autoregressive (AR) models to capture spatial-temporal dynamics of the temperature and wind velocity fields and offers a robust and accurate solution to the acoustic tomography problem.

This paper is organized as follows. Section 2 reviews the acoustic tomography problem formulation. The proposed acoustic tomography method is described in detail in Section 3. Finally, Section 4 shows the results of the proposed method.

2. PROBLEM FORMULATION

The travel time for an acoustic wave to propagate from a source to a receiver is a function of temperature,wind velocity (air flow) and humidity along the path [1, 2, 3]. However, the effect of humidity on the travel time is somehow negligible and hence is typically be ignored. In the absence of wind, an

This research was supported by the DoD Center for Geosciences/Atmospheric Research at Colorado State University under Cooperative Agreement W911NF-06-2-0015 with the Army Research Laboratory.

[1]Note: Throughout this paper "acoustic tomography" is used frequently instead "acoustic time-travel tomography".

acoustic wavefront propagates with Laplace sound speed [1], given by

$$c_L^2 = \gamma R_a T_{av}, \quad (1)$$

where $\gamma \approx 1.41$ denotes the ratio of specific heat capacities at constant pressure and volume, R_a is the universal gas constant for dry air and T_{av} is the acoustic virtual temperature which is related to the thermodynamic temperature T_{th}, as $T_{av} = T_{th}(1 + 0.511q)$, with q being the specific humidity defined as the ratio of water vapor to moist air.

In the field experiments though, wind velocity significantly impacts the time of arrivals and can be formulated as:

$$\mathbf{v}(\mathbf{r},t) = \alpha(\mathbf{r},t)cos(\theta(\mathbf{r},t))\mathbf{e}_x + \alpha(\mathbf{r},t)sin(\theta(\mathbf{r},t))\mathbf{e}_y, \quad (2)$$

where $\mathbf{e}_x$ and $\mathbf{e}_y$ are the unit vectors of a 2D-Cartesian coordinate system, $\mathbf{r} = x\mathbf{e}_x + y\mathbf{e}_y$ is the position vector of a point on the investigation area, and $\alpha(\mathbf{r},t)$ and $\theta(\mathbf{r},t)$ are magnitude and direction of the wind velocity at position $\mathbf{r}$ and time t, respectively. Therefore, the sound speed along the sound ray can be defined as:

$$c_{ray}(\mathbf{r},t) = \mathbf{s}.(c_L(\mathbf{r},t).\mathbf{n} + \mathbf{v}(\mathbf{r},t)), \quad (3)$$

where $\mathbf{s}$ and $\mathbf{n}$ denote the unit vectors in the direction of sound propagation and normal to the wavefront, respectively.

The straight-ray model for acoustic propagation which is the simplest model typically used in most literature is valid for sound propagation distances of few hundreds of meters, when the temperature and wind velocity fields are smooth and the speed of wind is much less than the Laplace sound speed c_L. For the straight-ray model, $\mathbf{s}$ and $\mathbf{n}$ are in the same direction and hence $\mathbf{s}.\mathbf{n} \approx 1$. However, in the presence of: (a) large temperature or wind velocity gradients; and (b) high wind speed, using the straight-ray model leads to non-unique solutions of the wind velocity field [4]. If time-synchronized acoustic signatures at various sensor nodes are available, one can use direction of arrival (DOA) estimation methods [6] to improve the accuracy of the wind velocity field reconstruction [4].

Assuming a straight-ray model for sound propagation, the sound speed along a propagation path can be written as:

$$c_{ray}(\mathbf{r},t) = c_L(\mathbf{r},t) + \mathbf{s}.\mathbf{v}(\mathbf{r},t). \quad (4)$$

Based on (4) which is a well-known relation for the effective sound speed, the travel time formula for the n'th path is defined as:

$$\tau_n(t) = \int_{L_n} \frac{\mathrm{d}l_n}{c_{ray}(\mathbf{r},t)} = \int_{L_n} \frac{\mathrm{d}l_n}{c_L(\mathbf{r},t) + \mathbf{s}_n.\mathbf{v}(\mathbf{r},t)}, \quad (5)$$

where the integration is along the n'th propagation path, L_n is the length of the n'th propagation path and $\mathbf{s}_n$ is the unit vector in its direction .

In order to be able to estimate the fields in the investigation area, almost all existing methods [1, 2, 3] discretize the investigation area, into grids and assume that $c_L(\mathbf{r},t)$ and $\mathbf{v}(\mathbf{r},t)$ are spatially constant in each grid. Using $I \times J$ grids, (5) can be discretize as:

$$\tau_n(t) = \Sigma_{i=1}^{I}\Sigma_{j=1}^{J} \frac{d_n(i,j)}{c_L([i,j],t) + \mathbf{s}_n.\mathbf{v}([i,j],t)}. \quad (6)$$

Here $d_n(i,j)$ is the distance n'th propagation path travels in the (i,j)'th cell, $c_L([i,j],t)$ and $\mathbf{v}([i,j],t)$ are the Laplace sound speed and the wind velocity vector in the (i,j)'th grid at time t, respectively and are demonstrated in Figure 1.

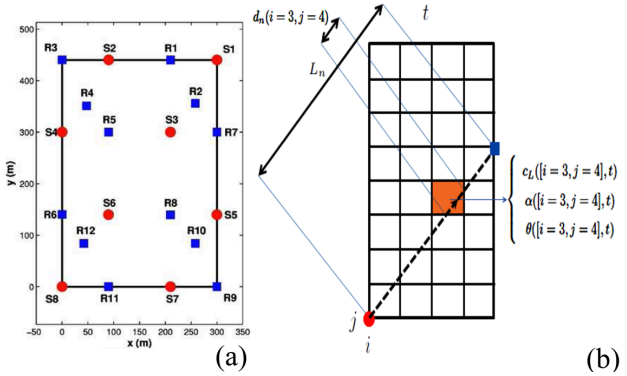

Fig. 1. (a) The layout of the STINHO field experiment (b) Discretization process

The term $\mathbf{s}_n.\mathbf{v}([i,j],t)$ in (6) can be written as:

$$\mathbf{s}_n.\mathbf{v}([i,j],t) = \alpha([i,j],t)cos(\theta([i,j],t))cos(\phi_n) + \alpha([i,j],t)sin(\theta([i,j],t))sin(\phi_n), \quad (7)$$

where $\alpha([i,j],t)$ and $\theta([i,j],t)$ are respectively the amplitude and the angle (with respect to $\mathbf{e}_x$) of wind velocity in the (i,j)th grid at time t and ϕ_n is the angle of the n'th propagation path with $\mathbf{e}_x$. The goal of acoustic tomography is then to find $c_L([i,j],t)$, $\alpha([i,j],t)$ and $\theta([i,j],t)$, for $i = 1,...,I$ and $j = 1,...,J$, given coordinates of the acoustic transmitters and receivers deployed in the field and the travel times between each transmitter and receiver, $\tau_n(t)$s, recorded for all propagation paths and at each snapshot t.

3. ACOUSTIC TOMOGRAPHY USING UKF METHOD

UKF employs unscented transform [5] to estimate the distribution of a posteriori state without the need for any linearization by propagating through the nonlinear functions [5].

Here, the Laplace sound speed, wind velocity amplitude and wind velocity angle at all grids are arranged to form the state vector.

$$\mathbf{x}_t = [\mathbf{c}_L(t)^T, \boldsymbol{\alpha}(t)^T, \boldsymbol{\theta}(t)^T]^T, \quad (8)$$

where $\mathbf{c}_L(t) = [c_L([1,1],t), c_L([1,2],t), ..., c_L([I,J],t)]^T$ is the column vector of the Laplace sound speeds at every grid, and similarly for $\boldsymbol{\alpha}(t)$ and $\boldsymbol{\theta}(t)$. The observation vector, $\mathbf{y}_t$, on the other hand, consists of time of arrival measurements for all acoustic propagation paths. That is, $\mathbf{y}_t = [\tau_1(t), ..., \tau_N(t)]^T$, where $\tau_i(t)$ is the travel time for the i'th path at snapshot t.

3.1. State Evolution Process

Since the fields don't change abruptly from one snapshot to the next, a reasonable model to capture the state dynamics is an autoregressive (AR) model. The adjacent neighbors at time $t-1$ are used as the support region for each grid at time t. For instance, the state evolution equation for the Laplace sound speed at time t is defined as follow

$$\mathbf{c}_L(t) \quad = \quad \mathrm{A}^{(c_L)}\mathbf{c}_L(t-1) + \mathbf{u}_{c_L}(t) \tag{9}$$

where $\mathbf{u}_{c_L}(t)$ is the column vector of the Laplace sound speed deriving process. Matrix $\mathrm{A}^{(c_L)}$ is a block Toeplitz matrix with Toeplitz blocks, and for the case of using a 4×8 grid it is defined as the right-stochastic (each row is normalized by the sum of the elements) of the matrix $\mathrm{A}'^{(c_L)}$ which is defined as,

$$\mathrm{A}'^{(c_L)} \triangleq \begin{bmatrix} \mathrm{B} & \mathrm{C} & \mathbf{0} & \mathbf{0} & \mathbf{0} & \mathbf{0} & \mathbf{0} & \mathbf{0} \\ \mathrm{C} & \mathrm{B} & \mathrm{C} & \mathbf{0} & \mathbf{0} & \mathbf{0} & \mathbf{0} & \mathbf{0} \\ \mathbf{0} & \mathrm{C} & \mathrm{B} & \mathrm{C} & \mathbf{0} & \mathbf{0} & \mathbf{0} & \mathbf{0} \\ \mathbf{0} & \mathbf{0} & \mathrm{C} & \mathrm{B} & \mathrm{C} & \mathbf{0} & \mathbf{0} & \mathbf{0} \\ \mathbf{0} & \mathbf{0} & \mathbf{0} & \mathrm{C} & \mathrm{B} & \mathrm{C} & \mathbf{0} & \mathbf{0} \\ \mathbf{0} & \mathbf{0} & \mathbf{0} & \mathbf{0} & \mathrm{C} & \mathrm{B} & \mathrm{C} & \mathbf{0} \\ \mathbf{0} & \mathbf{0} & \mathbf{0} & \mathbf{0} & \mathbf{0} & \mathrm{C} & \mathrm{B} & \mathrm{C} \\ \mathbf{0} & \mathbf{0} & \mathbf{0} & \mathbf{0} & \mathbf{0} & \mathbf{0} & \mathrm{C} & \mathrm{B} \end{bmatrix} \tag{10}$$

$$\mathrm{B} = \begin{bmatrix} \rho_0^{c_L} & \rho_1^{c_L} & 0 & 0 \\ \rho_1^{c_L} & \rho_0^{c_L} & \rho_1^{c_L} & 0 \\ 0 & \rho_1^{c_L} & \rho_0^{c_L} & \rho_1^{c_L} \\ 0 & 0 & \rho_1^{c_L} & \rho_0^{c_L} \end{bmatrix}, \mathrm{C} = \begin{bmatrix} \rho_1^{c_L} & \rho_2^{c_L} & 0 & 0 \\ \rho_2^{c_L} & \rho_1^{c_L} & \rho_2^{c_L} & 0 \\ 0 & \rho_2^{c_L} & \rho_1^{c_L} & \rho_2^{c_L} \\ 0 & 0 & \rho_2^{c_L} & \rho_1^{c_L} \end{bmatrix} \tag{11}$$

The AR coefficients $\rho_0^{c_L}$,$\rho_1^{c_L}$ and $\rho_2^{c_L}$ are estimated based on Yule-Walker method, using either training data set if in-situ measurements are available or assuming a specific spatial-temporal correlation structure [3] for each field. Similarly for $\boldsymbol{\alpha}(t)$ and $\boldsymbol{\theta}(t)$ we have

$$\begin{aligned} \boldsymbol{\alpha}(t) \quad &= \quad \mathrm{A}^{(\alpha)}\boldsymbol{\alpha}(t-1) + \mathbf{u}_\alpha(t) \\ \boldsymbol{\theta}(t) \quad &= \quad \mathrm{A}^{(\theta)}\boldsymbol{\theta}(t-1) + \mathbf{u}_\theta(t), \end{aligned} \tag{12}$$

here $\mathbf{u}_\alpha(t)$ and $\mathbf{u}_\theta(t)$ are, respectively the driving process for amplitude and the angle of wind velocity and matrices $\mathrm{A}^{(\alpha)}$ and $\mathrm{A}^{(\theta)}$ are calculated in a similar manner as $\mathrm{A}^{(c_L)}$. Note that the AR models are assumed to be decoupled from each other as the phenomena that generate them are independent. Combining these decoupled equations yields

$$\mathbf{x}_t \quad = \quad \mathrm{A}\mathbf{x}_{t-1} + \mathbf{u}_t, \tag{13}$$

where $\mathbf{u}_t = [\mathbf{u}_{c_L}(t)^T, \mathbf{u}_\alpha(t)^T, \mathbf{u}_\theta(t)^T]^T$ is the augmented deriving noise vector which is assumed to be Gaussian with zero mean and known covariance matrix R_u and matrix A is

$$\mathrm{A} = \begin{bmatrix} \mathrm{A}^{(c_L)} & \mathbf{0} & \mathbf{0} \\ \mathbf{0} & \mathrm{A}^{(\alpha)} & \mathbf{0} \\ \mathbf{0} & \mathbf{0} & \mathrm{A}^{(\theta)} \end{bmatrix}. \tag{14}$$

3.2. Observation Process

The relationship between state $\mathbf{x}_t$ and observation vector $\mathbf{y}_t$ at time t is given by (6) and (7) which is a nonlinear function of the state variables.

$$\mathbf{y}_t \quad = \quad H(\mathbf{x}_t) + \mathbf{v}_t, \tag{15}$$

where $\mathbf{v}_t$ stands for measurement noise caused by such things as,(i) errors inherent in the griding process (ii) error in measuring the time of arrivals, and (iii) sensor location error and it is assumed to be a Gaussian random vector with zero mean and known covariance matrix, R_v. The most dominant source for this error is (i). The nonlinear function $H(\mathbf{x}_t)$ is explicitly defined as

$$H(\mathbf{x}_t) = \begin{bmatrix} \Sigma_{i=1}^{I}\Sigma_{j=1}^{J} \frac{d_1(i,j)}{c_L([i,j],t)+\mathbf{s}_1.\mathbf{v}([i,j],t)} \\ \vdots \\ \Sigma_{i=1}^{I}\Sigma_{j=1}^{J} \frac{d_N(i,j)}{c_L([i,j],t)+\mathbf{s}_N.\mathbf{v}([i,j],t)} \end{bmatrix} \tag{16}$$

3.3. Fixed-Point Iterative UKF Equations

In the case of large uncertainty in the choice of the initial error covariance matrix $P_{0|0}$ and weak observability of the system, UKF exhibits slow convergence problem and poor state estimation accuracy. Iterated UKF [7] is a more robust version of UKF which not only iterates on every snapshot t but also performs fixed-point iteration at each fixed snapshot to get a more robust and accurate state estimates.

To apply fixed-point iterative UKF to any nonlinear state estimation process, one needs to generate estimates of covariance matrices R_u and R_v for the deriving noise and measurement noise, respectively. The covariance matrix R_u is generally estimated using either training data or assuming a spatial-temporal correlation as mentioned before. The covariance matrix R_v , on the other hand, can be estimated from typical measurement data and the error in the measurement devices. Given these matrices and defining $x_{k|k}(t)$ to be the state estimate at k'th iteration on snapshot t, the fixed-point iterative UKF steps for $k \in [0, K]$ iterations on each snapshot are:

3.3.1. Initialization

Fixed-point iterative UKF starts by initializing the state vector estimate $\hat{\mathbf{x}}_{K|K}(0)$ (i.e. estimate of state vector, given observation at time $t = 0$). Additionally the corresponding state error covariance matrix $\mathrm{P}_{K|K}(0)$ is initialized with an identity matrix. The initial state vector at snapshot t is then set to be $\hat{\mathbf{x}}_{0|0}(t) = \hat{\mathbf{x}}_{K|K}(t-1)$ and the corresponding covariance matrix $\mathrm{P}_{0|0}(t) = \mathrm{P}_{K|K}(t-1)$.

3.3.2. Generating Initial Sigma Points

Sigma points are $2L+1$ point masses to approximate the input distribution. Using the initial estimates $\hat{\mathbf{x}}_{k-1|k-1}(t)$ and $P_{k-1|k-1}(t)$ for the k'th iteration at time t, the sigma points are calculated as follows

$$\begin{aligned}\boldsymbol{\chi}_{0,k-1|k-1}(t) &= \hat{\mathbf{x}}_{k-1|k-1}(t)\\ \boldsymbol{\chi}_{i,k-1|k-1}(t) &= \hat{\mathbf{x}}_{k-1|k-1}(t)+\gamma\sqrt{\mathrm{P}_{k-1|k-1}(t)}_{[i]}\\ \boldsymbol{\chi}_{L+i,k-1|k-1}(t) &= \hat{\mathbf{x}}_{k-1|k-1}(t)-\gamma\sqrt{\mathrm{P}_{k-1|k-1}(t)}_{[i]},\end{aligned} \quad (17)$$

for $i=1\ldots L$, where $\gamma\approx\varrho\sqrt{L}$ is a scaling parameter and ϱ determines the spread of sigma points around $\hat{\mathbf{x}}_{k-1|k-1}(t)$ and $\sqrt{\mathrm{P}_{k-1|k-1}(t)}_{[i]}$ is the i'th column of the Cholesky factor of $P_{k-1|k-1}(t)$.

3.3.3. A Priori State Estimation

The initial sigma points are transformed through the state evolution equation (13).

$$\boldsymbol{\chi}^{*}_{i,k|k-1}(t)=\mathrm{A}\boldsymbol{\chi}_{i,k-1|k-1}(t),\ \ i=0,\ldots,2L \quad (18)$$

A weighted sum of these transformed sigma points is calculated to estimate the a priori state, $\hat{\mathbf{x}}_{k|k-1}(t)$, and covariance matrix, $\mathrm{P}_{k|k-1}(t)$:

$$\hat{\mathbf{x}}_{k|k-1}(t)=\sum_{i=0}^{2L}W_i^{(m)}\boldsymbol{\chi}^{*}_{i,k|k-1}(t), \quad (19)$$

$$\begin{aligned}\mathrm{P}_{k|k-1}(t)=\mathrm{R}_u+\sum_{i=0}^{2L}(W_i^{(c)}[\boldsymbol{\chi}^{*}_{i,k|k-1}(t)-\hat{\mathbf{x}}_{k|k-1}(t)]\\ [\boldsymbol{\chi}^{*}_{i,k|k-1}(t)-\hat{\mathbf{x}}_{k|k-1}(t)]^T\end{aligned} \quad (20)$$

where the weights $W_i^{(m)}$s and $W_i^{(c)}$s are [8] as $W_0^{(m)}=\frac{\lambda}{\lambda+L}$, $W_0^{(c)}=\frac{\lambda}{\lambda+L}+(1-\varrho^2+\beta)$, and $W_i^{(m)}=W_i^{(c)}=\frac{1}{2(L+\lambda)}$ for $i=1,\ldots,2L$ with β being a constant used to incorporate prior knowledge of the distribution of the state vector and is set to $\beta=2$ for Gaussian distributions.

3.3.4. Covariance Matrices Computation

New sigma points are calculated based on $\hat{\mathbf{x}}_{k|k-1}(t)$ and $\mathrm{P}_{k|k-1}(t)$ to be fed into the nonlinear function $H(.)$ in order to estimate the measurement update, $\hat{\mathbf{y}}_{k|k-1}(t)$.

$$\begin{aligned}\boldsymbol{\chi}_{0,k|k-1}(t) &= \hat{\mathbf{x}}_{k|k-1}(t)\\ \boldsymbol{\chi}_{i,k|k-1}(t) &= \hat{\mathbf{x}}_{k|k-1}(t)+\gamma\sqrt{P_{k|k-1}(t)}_{[i]}\\ \boldsymbol{\chi}_{L+i,k|k-1}(t) &= \hat{\mathbf{x}}_{k|k-1}(t)-\gamma\sqrt{P_{k|k-1}(t)}_{[i]}\end{aligned} \quad (21)$$

for $i=1\ldots L$.

The new sigma points are transformed through the nonlinear observation process(15), to yield:

$$\boldsymbol{\Upsilon}_{i,k|k-1}(t)=H(\boldsymbol{\chi}_{i,k|k-1}(t))\ \ i=0,\ldots,2L. \quad (22)$$

The weighted sum, covariance matrix and cross-covariance matrix of the measurement vector are calculated as

$$\hat{\mathbf{y}}_{k|k-1}(t) = \sum_{i=0}^{2L}W_i^{(m)}\boldsymbol{\Upsilon}_{i,k|k-1}(t) \quad (23)$$

$$\begin{aligned}\mathrm{P}_{yy,k}(t) = \mathrm{R}_v+\sum_{i=0}^{2L}(W_i^{(c)}[\boldsymbol{\Upsilon}_{i,k|k-1}(t)-\hat{\mathbf{y}}_{k|k-1}(t)]\\ [\boldsymbol{\Upsilon}_{i,k|k-1}(t)-\hat{\mathbf{y}}_{k|k-1}(t)]^T)\end{aligned} \quad (24)$$

$$\begin{aligned}\mathrm{P}_{xy,k}(t) = \sum_{i=0}^{2L}(W_i^{(c)}[\boldsymbol{\chi}_{i,k|k-1}(t)-\hat{\mathbf{x}}_{k|k-1}(t)]\\ [\boldsymbol{\Upsilon}_{i,k|k-1}(t)-\hat{\mathbf{y}}_{k|k-1}(t)]^T)\end{aligned} \quad (25)$$

3.3.5. Kalman Gain Computation and A Posteriori State Estimation

These are used to generate the Kalman gain $\mathbf{K}_k(t)$, a posteriori state vector $\hat{\mathbf{x}}_{k|k}(t)$ and error covariance matrix $\mathrm{P}_{k|k}(t)$ estimations:

$$\mathbf{K}_k(t) = \mathrm{P}_{xy,k}(t)\mathrm{P}^{-1}_{yy,k}(t) \quad (26)$$

$$\hat{\mathbf{x}}_{k|k}(t) = \hat{\mathbf{x}}_{k|k-1}(t)+\mathbf{K}_k(t)(\mathbf{y}_t-\hat{\mathbf{y}}_{k|k-1}(t)) \quad (27)$$

$$\mathrm{P}_{k|k}(t) = \mathrm{P}_{k|k-1}(t)-\mathbf{K}_k(t)\mathrm{P}_{yy,k}(t)\mathbf{K}_k^T(t) \quad (28)$$

3.3.6. Iteration Step

If $k<K$ then the algorithm proceeds to the next iteration $k+1$ on the fixed snapshot t and redo steps 2 to 5. But if $k=K$ then it proceeds in time $t+1$ and uses the estimated state and error covariance matrix at time t as the initial values for time $t+1$, $\hat{\mathbf{x}}_{0|0}(t+1)=\hat{\mathbf{x}}_{K|K}(t)$ and $P_{0|0}(t+1)=P_{K|K}(t)$ and jumps to step 2.

4. RESULTS

In order to test our proposed UKF-based algorithm a data set was acquired from the University of Leipzig, collected at the Meteorological Observatory, Lindenberg, Germany, as part of the STINHO project [9]. However, the lack of sufficient in situ measurements for a complete evaluation of the developed method motivated us to construct a synthetic but realistic data set. The synthetic data was generated based on fractal Brownian motion (fBm) model [10] for wind velocity and temperature fields in the investigation area. To be more realistic the field size and the sensor locations were chosen to be the same as those in the STINHO experiment.

Figure 1 shows the layout of investigation field and the locations of the virtual receivers and transmitters indicated by R_i and S_i, respectively. The field is of the size $300m\times 440m$ with 8 transmitters and 12 receivers. The synthetic data is generated for 500 subsequent snapshots of wind velocity and temperature fields with spatial resolution of one meter and temporal resolution of 12 seconds. Note that this choice for resolution is chosen arbitrarily and can be changed. The time of arrival for each sound ray path is then calculated using (15) at each snapshot, choosing $\mathbf{v}_t$ to be a white Gaussian process

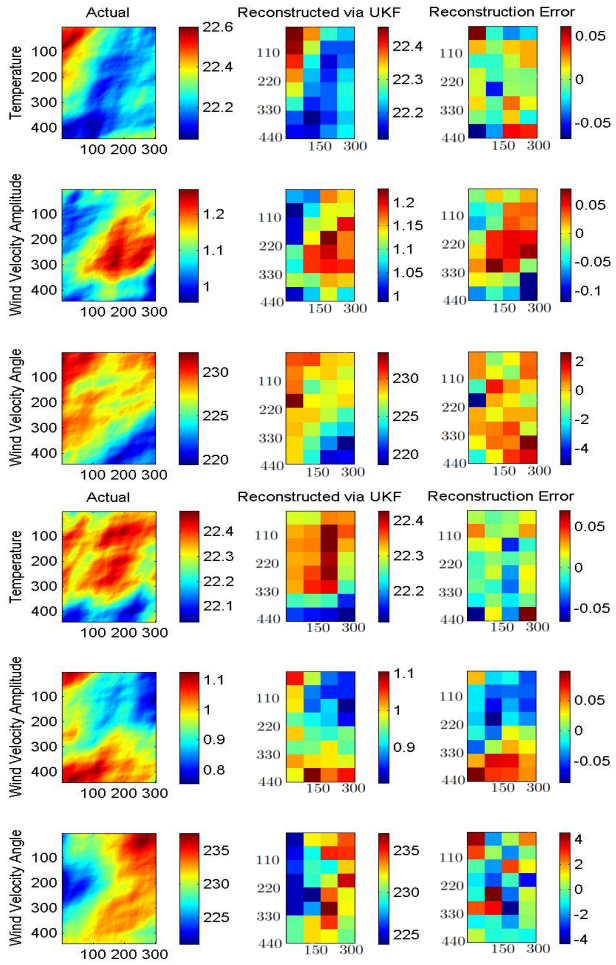

Fig. 2. Field reconstruction for snapshots 50 (top) and 150 (bottom).

with the variance $\sigma^2 = 0.01$. This variance is chosen to fit the uncertainty of measurements reported in [9] which is 0.3 millisecond for each measurement.

The first 5 snapshots of the synthesized data (1 minute worth of synthesized data) were used as the training data to estimate the AR model coefficients and the covariance matrices R_u and R_v. Using the Yule-Walker method the 3-D AR coefficients are estimated and used to reconstruct the temperature, wind velocity amplitude and angle fields using steps 1-5 of the iterated UKF presented. Figure 2 illustrates the results of the field reconstruction for snapshots 50 and 150. The reconstruction cells are of the size $75m \times 55m$, and the reconstruction error shows the difference between actual fields (averaged at the grids) and the reconstructions. As can be seen, the UKF-based method provides accurate results. The computation time for the iterated UKF with $K = 3$ at every snapshot is approximately 5sec on a computer with Intel Core i7 CPU, $12.0GB$ RAM, and $64bit$ operating system. Thus, the proposed UKF-based method is highly computationally efficient, ideally suited for applications where near real-time state estimation is required. Other unique benefits include tracking ability of the fields, robustness to measurement noise, and reconstruction accuracy when compared to other statistical-based acoustic tomography methods.

5. REFERENCES

[1] D. K. Wilson and D. W. Thomson, "Acoustic tomographic monitoring of the atmospheric surface layer," *Atmospheric and Oceanic Technology*, vol. 11, pp. 751–769, June 1994.

[2] K. Arnold, A. Ziemann, A. Raabe, and G. Spindler, "Acoustic tomography and conventional meteorological measurements over heterogeneous surfaces," *Meteorology and Atmospheric Physics*, vol. 85, pp. 175–186, 2004.

[3] S. N. Vecherin, V. E. Ostashev, G. H. Goedecke, D. K. Wilson, and A. G. Voronovich, "Time-dependent stochastic inversion in acoustic travel-time tomography of the atmosphere," *The Journal of the Acoustical Society of America*, vol. 119, pp. 2579–2588, May 2006.

[4] I. Jovanovic, "Acoustic tomography for scalar and vector fields : theory and application to temperature and wind estimation," *Journal of Atmospheric and Oceanic Technology*, pp. 1–15, 2009.

[5] S. J Julier and J. K Uhlmann, "Unscented filtering and nonlinear estimation," *Proceedings of the IEEE*, vol. 92, pp. 401–422, 2004.

[6] H L Van Trees, *Optimum Array Processing*, vol. Part IV, Wiley-Interscience, 2002.

[7] R. Zhan and J. Wan, "Iterated unscented Kalman filter for passive target tracking," *Aerospace and Electronic Systems, IEEE Transactions on*, vol. 43, pp. 1155 –1163, July 2007.

[8] E. A. Wan and R. V. Merwe, "The unscented Kalman filter," in *Kalman filtering and neural networks*, S. S. Haykin, Ed., chapter 7, pp. 221–277. John Wiley and Sons, New York, US, 2001.

[9] A. Raabe, A. Klaus, A. Ziemann, M. Schroter, S. Raasch, J. Bange, P. Zittel, T. Spieb, T. Foken, M. Gockede, F. Beyrich, and J. P. Leps, "STINHO, structure of turbulent transport under inhomogeneous surface conditions," *Meteorologische*, vol. 14, pp. 315–327, 2005.

[10] O. Khorloo, Z. Gunjee, and B. Sosorbaram, "Wind field synthesis for animating wind-induced vibration," *The International Journal of Virtual Reality*, vol. 10, pp. 53–60, February 2011.